Journal of Hydrology 517 (2014) 269–283

Contents lists available at ScienceDirect

Journal of Hydrology

journal homepage: www.elsevier.com/locate/jhydrol

Regional scale impact of tidal forcing on groundwater flow in unconfined coastal aquifers

P.S. Pauw [a,b,*], G.H.P. Oude Essink [a], A. Leijnse [b], A. Vandenbohede [d], J. Groen [c], S.E.A.T.M. van der Zee [b]

[a] Deltares, Department of Soil and Groundwater, P.O. Box 85467, 3508 AL Utrecht, The Netherlands
[b] Wageningen University, Environmental Sciences Group, Soil Physics and Land Management, P.O. Box 47, 6700 AA Wageningen, The Netherlands
[c] VU University Amsterdam, Faculty of Earth and Life Sciences, Hydrology and Geo-Environmental Sciences, Boelelaan 1085, 1081 HV Amsterdam, The Netherlands
[d] University of Ghent, Department of Geology and Soil Science, Krijgslaan 281 S8, B-9000 Ghent, Belgium

ARTICLE INFO

Article history:
Received 2 September 2013
Received in revised form 4 May 2014
Accepted 15 May 2014
Available online 24 May 2014
This manuscript was handled by Peter K. Kitanidis, Editor-in-Chief, with the assistance of Todd C. Rasmussen, Associate Editor

Keywords:
Tidal forcing
Regional groundwater flow
Unconfined coastal aquifer
Overheight
Variable density flow

SUMMARY

This paper considers the impact of tidal forcing on regional groundwater flow in an unconfined coastal aquifer. Numerical models are used to quantify this impact for a wide range of hydrogeological conditions. Both a shallow and a deep aquifer are investigated with regard to three dimensionless parameter groups that determine the groundwater flow to a large extent. Analytical expressions are presented that allow for a quick estimate of the regional scale effect of tidal forcing under the same conditions as used in the numerical models.

Quantitatively, the results in this paper are complementary to previous studies by taking into account variable density groundwater flow, dispersive salt transport and a seepage face in the intertidal area. Qualitatively, the results are in line with previous investigations. The time-averaged hydraulic head at the high tide mark increases upon a decrease of each of the three considered dimensionless parameter groups: R (including the ratio of the hydraulic conductivity and the precipitation excess), α (the slope of the intertidal area) and A_L (the ratio of the width of the fresh water lens and the tidal amplitude). The relative change of the location and the hydraulic head of the groundwater divide, which together characterize regional groundwater flow, increase as α and A_L decrease, but decrease as R decreases. The difference between the analytical solutions and numerical results is small. Therefore, the presented analytical solutions can be used to estimate the bias that is introduced in a numerical model if tidal forcing is neglected. The results should be used with caution in case of significant wave forcing, as this was not considered.

1. Introduction

Numerical models are widely used to quantify groundwater flow and salt transport in real-world coastal aquifers (Oude Essink et al., 2010; Sulzbacher et al., 2012; Vandenbohede et al., 2008). Assumptions and simplifications are often needed in these models to cope with computational limitations. A common assumption in regional scale models is to neglect forcing from the sea, such as tides, waves and storm events. Several studies have shown that this assumption leads to underestimated heads near the shore (Cartwright, 2004; Kang, 1995; Nielsen, 1990; Turner et al., 1995). However, the question that remains is: how significant is this effect on a regional scale?

Forcing from the sea results in (periodic) inundation of the intertidal area (Fig. 1b). The zone where groundwater discharges during low tide is generally smaller than the inundation zone during high tide. Consequently, time-averaged groundwater levels are elevated compared to a situation where there is no forcing from the sea (Fig. 2) (Lebbe, 1983; Nielsen, 1990; Vandenbohede and Lebbe, 2005). This effect increases as the slope of the intertidal area and the hydraulic conductivity of the intertidal sediments decreases (Horn, 2006; Nielsen, 1990; Turner et al., 1995) and also influences the groundwater salinity distribution below the intertidal area (Ataieashtiani et al., 1999; Cartwright, 2004; Lebbe, 1983; Robinson et al., 2006; Thorn and Urish, 2012).

Previous related studies have mainly considered the near-shore region, where the forcing on the groundwater levels is most pronounced (Nielsen, 1990; Robinson et al., 2007; Turner et al., 1995). Few studies have indicated the regional scale effects

* Corresponding author at: Deltares, Department of Soil and Groundwater, P.O. Box 85467, 3508 AL Utrecht, The Netherlands. Tel.: +31 623786887.
E-mail addresses: pieter.pauw@deltares.nl (P.S. Pauw), gualbert.oudeessink@deltares.nl (G.H.P. Oude Essink), toon.leijnse@wur.nl (A. Leijnse), alexander.vandenbohede@ugent.be (A. Vandenbohede), koos.groen@vu.nl (J. Groen), sjoerd.vanderzee@wur.nl (S.E.A.T.M. van der Zee).

http://dx.doi.org/10.1016/j.jhydrol.2014.05.042
0022-1694/

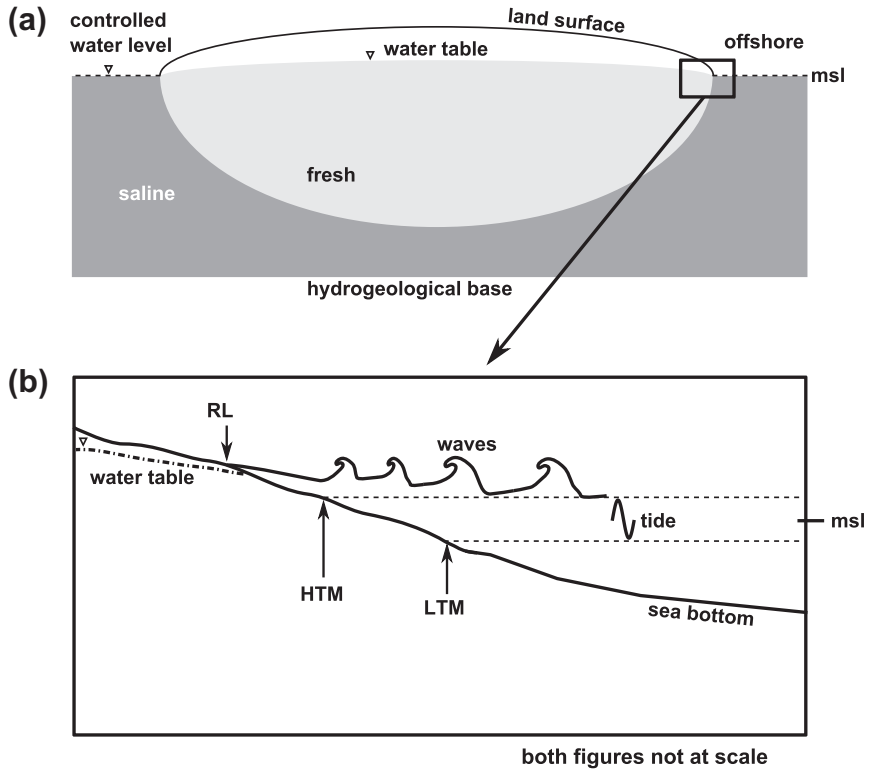

Fig. 1. (a) Conceptual cross section of the groundwater salinity distribution of a freshwater lens on a regional scale in case of a constant mean sea level. Note that in reality a transition zone between fresh and saline groundwater exists. (b) Forcing on the groundwater below the beach by waves and tides. Infiltration of seawater occurs up to the upper limit of the wave run-up at high tide (RL). In case waves are dominant, RL is situated higher and further inland than the high tide mark (HTM). A comparable effect occurs during low tide regarding the low tide mark (LTM). This wave run-up effect can have a large influence on the time-averaged groundwater levels Nielsen (1999). Note that the groundwater salinity distribution is not shown. (b) was largely adopted from a more detailed figure in Nielsen (1999) (by permission).

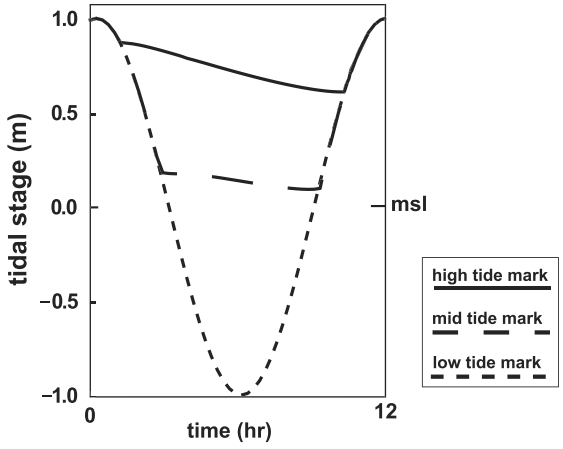

Fig. 2. Conceptual behavior of groundwater levels in an intertidal area around the low tide mark (LTM), the high tide mark (HTM) and in between them (mid tide mark; MTM), over one tidal cycle in case of tidal forcing. The resistance to drainage of the intertidal area is higher than the resistance to infiltration. To obtain a balance between inflow and outflow over a tidal cycle, the time-averaged groundwater levels inland of LTM are higher than mean sea level.

(Nielsen, 1999; Urish and Melih, 1989), despite the potential influence on the location of the groundwater divide and, hence, the amount of water that discharges to the hinterland and to the sea. An important reason to neglect the highly-dynamic processes in numerical models is the high computational effort required. Some regional scale model studies have accounted for the forcing from the sea, by using time-averaged hydraulic heads in the intertidal area that were either based on field observations or manual calibration (Vandenbohede and Lebbe, 2005; Werner and Gallagher, 2006).

The objective of this paper is to provide an estimate of the regional scale effect of tides on hydraulic heads in an unconfined coastal aquifer with an intertidal area. It is important to note here that, depending on the local conditions, waves and storm events can also have a significant, or even larger contribution on the hydraulic heads than tides (Nielsen, 1999) (Fig. 1b) but that this is not considered here. In case waves have a significant influence, the results in this paper should be used with caution.

The term overheight (Nielsen, 1990) is used to indicate the underestimated hydraulic heads in a model where tides are neglected. More specifically, overheight is defined here as the difference in the computed water table between a model where tides are neglected, and a model where tides are taken into account. The influence of tides on both the location and hydraulic head at the groundwater divide is jointly referred to as regional scale overheight. Using numerical models, regional scale overheight is determined for the following hydrogeological cases:

- *Fresh water lens in a deep aquifer.* In this case, the unconfined aquifer is isotropic, homogeneous and the hydrogeological base is deep enough to accommodate the entire fresh water body (Fig. 1a).
- *Fresh water lens in a shallow aquifer.* This case is analogous to the case of a fresh water lens in a deep aquifer, except that the hydrogeological base corresponds with the maximum depth of the fresh - saline transition zone.
- *Fresh water lens in a heterogeneous subsurface.* This case consists of an example of a layered coastal aquifer system in the Netherlands and serves as an illustration of how to use the findings from the cases of the deep and shallow aquifer in a more complex subsurface.

For these cases, the fresh water lens is subjected to tidal forcing on only one side (i.e., the seaward side), which may for example be the case in coastal barriers. A shallow aquifer is considered, as Nielsen (1990) showed that the depth of the aquifer also influences the overheight. Within all the cases, a wide range of hydrogeological parameters is considered that influence the groundwater flow in the intertidal area and the adjacent aquifer. Analytical solutions are derived for the same conditions and are compared with the numerical model results to investigate their suitability for a simple approximation of the regional scale overheight.

2. Material and methods

2.1. SEAWAT

SEAWAT (Langevin et al., 2007) was used to solve the following partial differential equation for variable density groundwater flow in all numerical simulations:

$$\nabla \cdot \left[\rho \mathbf{K_0}\left(\nabla h_f + \frac{\rho - \rho_f}{\rho_f}\nabla z\right)\right] = \rho S_s \frac{\partial h_f}{\partial t} + \theta \frac{d\rho}{dC}\frac{dC}{dt} - \rho_{ss} q_{ss} \quad (1)$$

where ρ is the density of the fluid [M L^{-3}], $\mathbf{K_0}$ is the hydraulic conductivity tensor [L T^{-1}], h_f is the freshwater head [L], z is the vertical coordinate [L], ρ_f is the density of fresh water [M L^{-3}], S_s is the specific storage coefficient [L^{-1}], t is the time [T], θ is the effective porosity [], C is the concentration [M L^{-3}], ρ_{ss} is the density of the sink or source [M L^{-3}] and q_{ss} is the sink and source term [T^{-1}]. It was assumed that $\mathbf{K_0}$ is isotropic, that the density of fresh water is ρ_f is 1000 kg m^{-3} and that the maximum density of the water ρ_s is 1025 kg m^{-3}. A linear equation of state was used to calculate fluid density from concentration, whereby it was assumed that only salt concentration influences fluid density:

$$\rho = \rho_f + \frac{d\rho}{dC}C \quad (2)$$

Relative salt concentrations were used, ranging from 0 (concentration of fresh water) to 1 (concentration of sea water). Hence, $\frac{d\rho}{dC}$ equals 25.

The govering equation for salt transport in the simulations was:

$$\frac{d(\theta C)}{dt} = \nabla \cdot (\theta \mathbf{D} \cdot \nabla C) - \nabla \cdot (\mathbf{q}C) - q_{ss}C_{ss} \quad (3)$$

where $\mathbf{D}$ is the hydrodynamic dispersion tensor [L^2 T^{-1}], $\mathbf{q}$ is the specific discharge vector [L T^{-1}] and C_{ss} is the source and sink concentration [M L^{-3}].

In all analyses, the groundwater flow equation and the dispersion term of the salt transport equation were formulated using a cell-centered finite difference scheme. The groundwater flow equation was solved using the PCG package (Hill, 1990). The non-advective part of the salt transport equation was solved using the GCG solver (Zheng and Wang, 1999). The advection term $-\nabla \cdot (\mathbf{q}C)$ was formulated by a Lagrangian scheme and solved using the MOC solver with a relatively small Courant number (0.1) and a minimum number of 9 and a maximum number of 54 particles per cell.

2.2. Boundary conditions

The modeling of periodic groundwater flow in a regional scale model domain requires a high computational effort. To reduce the computational effort, a step-wise procedure was used to compute the overheight:

- **Constant mean sea level (CMSL) model**. (Fig. 3a) First, the development of a fresh water lens in an initially saline domain (with concentration $C = 1$) was simulated using constant boundary conditions. The hydraulic head in the offshore region S is equal to mean sea level, whereby the water flowing into the model domain has a concentration C of 1. In the hinterland region P, the water level is controlled with level h_P, again having an inflow concentration $C = 1$. In the region L, a recharge flux was applied with concentration $C = 0$. The simulations were ended when the total salt mass in the model reached a constant value.
- **Periodic sea level (PSL) model**. (Fig. 3b) The result (i.e., concentrations and hydraulic heads) of the CMSL model is the initial condition for the periodic sea level model. The differences compared to the CMSL model are the boundary conditions in the intertidal area (B) and the offshore region (S), where a tidal boundary condition was applied. The simulations were ended when the time-averaged hydraulic heads (measured over one tidal cycle) and salt concentration in the intertidal area reached a constant value.
- **Time-averaged sea level model (TASL) model**. (Fig. 3a) The result of the periodic sea level model is the initial condition for the time-averaged sea level model. In this model, constant boundary conditions were applied, similar as in the constant mean sea level model. In the intertidal area and offshore regions a constant head boundary condition was applied based on the time-averaged hydraulic heads (measured over one tidal cycle) of the periodic sea level model with concentration $C = 1$. The simulations were ended when the time-averaged head at the groundwater divide and the total mass in the model reached a constant value.

The regional scale overheight was computed from the difference in hydraulic head between the CMSL and TASL models, whereby the hydraulic head was analyzed at $x = 0.5L$. In order to validate this step-wise approach, the TASL model was compared with a model wherein only periodic sea level was simulated. This model is referred to as 'step-wise validation model'. The boundary conditions of the step-wise validation model are equal to the ones used in the PSL model, but the initial condition for this model is a saline domain with $C = 1$. The step-wise validation model was ended when the time-averaged heads in the model reached a constant value.

The tidal boundary condition in the intertidal area in the periodic sea level models consists of head-dependent flux boundary cells. The GHB-DRN (General Head Boundary – Drain) approach described by Mulligan et al. (2011) was used for this purpose. When, for the cells representing the surface of the intertidal area, the hydraulic head in the intertidal area is lower than the sea level, inflow from a GHB cell occurs with an inflow concentration of 1. When the hydraulic head is higher than the sea level and higher than the surface elevation of the intertidal area, there is outflow to a DRN cell. For further details, the reader is referred to Mulligan et al. (2011).

In the intertidal area, the maximum horizontal length of the cells was 5 m and the maximum thickness of the layers was 0.2 m. This is comparable with the number of cells Mulligan et al. (2011) used for discretizing the intertidal area. The cell size gradually increases away from the intertidal area to maximum values of 50 m for the horizontal and 5 m for the vertical dimension. Using stress periods of 15 min and 1-min long flow and solute transport time steps, the following general form of the tidal oscillation was discretized:

$$h(t) = h_0 + A\sin(\omega t - \phi) \quad (4)$$

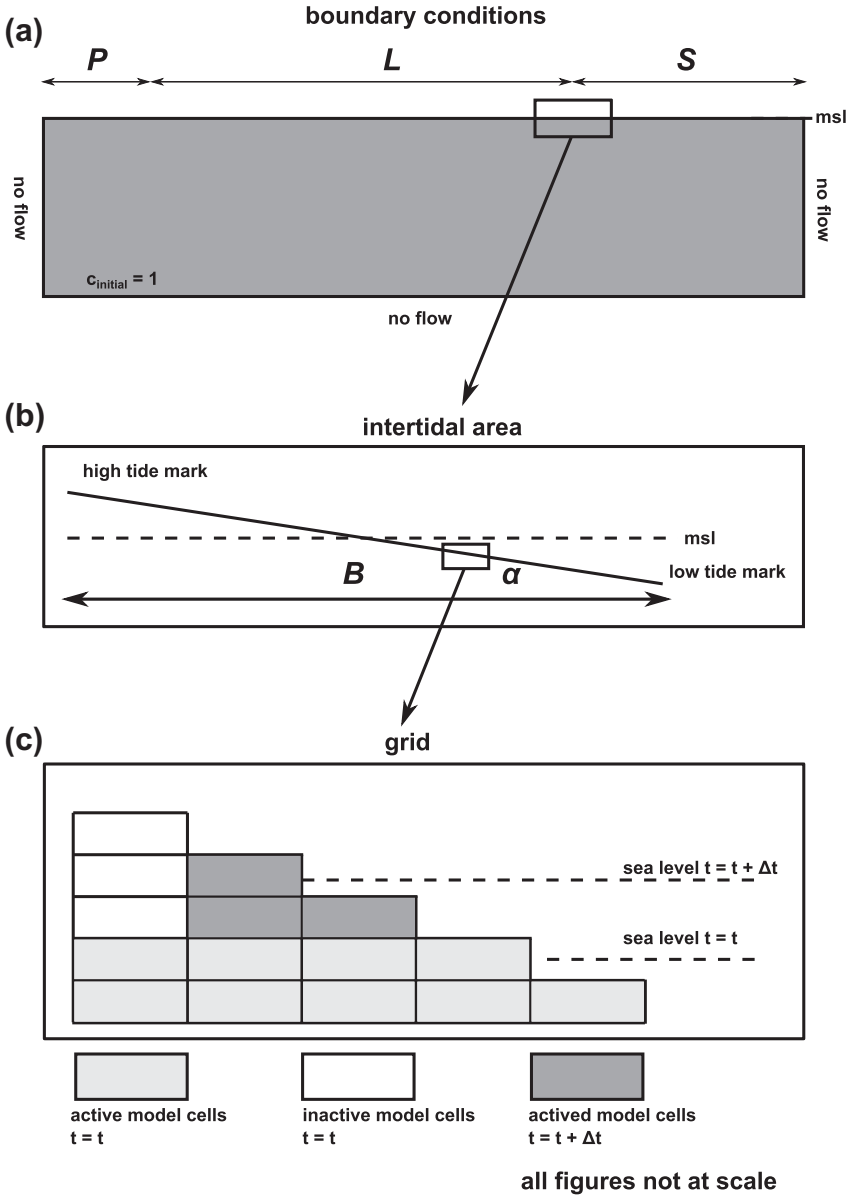

Fig. 3. (a) Boundary conditions of the constant mean sea level (CMSL) model. (b) Boundary conditions of the periodic sea level (PSL) model. α is the slope of the intertidal area, B is the width of the intertidal area. (c) The GHB-DRN tidal boundary condition (Mulligan et al., 2011), with the method for a correct timing of the tidal signal in the intertidal area.

where $h(t)$ is the sea level at time = t, h_0 is the reference hydraulic head (mean sea level), A is the tidal amplitude [L], ω is the frequency [T^{-1}] ($2\pi T^{-1}$, where T is the period [T]) and ϕ is the phase shift []. The effect of waves, spring and neap tides and wind effects on the water level were not considered. The terms 'tidal forcing' and 'tides' (a result of tidal forcing) therefore refer to diurnal variations in this paper.

The original GHB-DRN tidal boundary approach of Mulligan et al. (2011), only prescribes the boundary condition for the uppermost cells that represent the surface of the intertidal area. If the slope of the intertidal area is small and the hydraulic conductivity of the intertidal sediment is large (Table 1), a relatively large number of cells fall dry during falling tide (i.e., they become inactive in the simulation). Consequently, upon inundation of the intertidal area during rising tide, a delay of the tidal signal occurs. This can be attributed to the method of activating the inactive cells again; cells are allowed to be wetted only from below, as wetting from the horizontally adjacent cells leads to non-convergence of the flow solution (Mulligan et al., 2011). Therefore, the GHB boundary condition was prescribed for one stress period at the semi-saturated cell and across all cells that fall dry during ebb, as soon as inundation of that cell occured due to the rising water level

Table 1
Parameters used in the case of the fresh water lens in a deep aquifer. '(ref)' refers to the reference value.

Dimensionless group	Parameter values	Group value
R	K = 5 m d^{-1}, N = 0.002 m d^{-1}	62.5
R (ref)	K = 10 m d^{-1}, N = 0.001 m d^{-1}	250
R	K = 20 m d^{-1}, N = 0.0005 m d^{-1}	1000
α	A = 1 m, B = 200 m	0.01
α	A = 1 m, B = 100 m	0.02
α (ref)	A = 1 m, B = 50 m	0.04
α	A = 1 m, B = 25 m	0.08
α	A = 1 m, B = 20 m	0.10
A_L	L = 1000 m, A = 2.0 m	500
A_L	L = 1600 m, A = 1.6 m	1000
A_L (ref)	L = 2000 m, A = 1.0 m	2000
A_L	L = 3200 m, A = 0.8 m	4000
A_L	L = 4000 m, A = 0.5 m	8000

(Fig. 3c). This approach effectively assumes that the saturation of the unsaturated zone is instantaneous, and that the vertical downward flow of infiltrating seawater is not associated with a large head gradient. For implementation, this approach means that one has to know the number of desaturated cells beforehand. Since this is not possible to determine a priori, this was done by trial and error for each model simulation. The forced activation of cells allows for the use of a relatively high (−0.1, or 10% of the cell thickness and only wetting from below) WETDRY parameter of the BCF package. As a result, no problems with the convergence of the flow solution were encountered.

To justify this approach, a comparison was made with a simulation using the recently developed MODFLOW-NWT code (Niswonger et al., 2011). MODFLOW-NWT allows for a robust simulation of intertidal groundwater flow. Density variations were ignored and salt transport was not simulated. The results indicate a correct timing of the tidal signal, and negligible differences in hydraulic heads and fluxes between the models. Results of this analysis are omitted for brevity of this paper.

2.3. Constant model parameters

In all the analyses, the slope of the intertidal area is constant and the groundwater recharge is constant in time and does not vary spatially. In addition, the following parameters were kept constant: ratio of the horizontal and vertical hydraulic conductivity (1), the specific storage coefficient ($10^{-4}\,m^{-1}$), specific yield (0.25), effective porosity (0.35), longitudinal dispersivity (0.25 m) and transversal dispersivity (0.025 m). The dispersivity values in this study compare well with previous related modeling work on submarine groundwater discharge (Mulligan et al., 2011; Robinson et al., 2007; Vandenbohede and Lebbe, 2005) and macro dispersivities found by e.g., Gelhar et al. (1992) and Kaleris (2006). Lebbe (1999) and Van Meir (2001) found dispersivity values from regression modeling of field data that were about three times lower than the values is this paper, in a coastal aquifer of well-sorted medium to fine-medium sands. As will be shown further, the dispersivity values result in a relatively small mixing zone and in minor differences with the corresponding analytical solution that ignores dispersion. For a more detailed elaboration of dispersivity values in comparable coastal settings as in this paper, the reader is referred to Eeman et al. (2012).

2.4. Fresh water lens in the deep aquifer

A dimensional analysis of governing equations and boundary conditions for the case of the fresh water lens in the deep aquifer served as a basis for the variation of parameters, to enhance insight and efficiency. The parameter values are characteristic for regional scale freshwater lenses found in many low lying coastal aquifers world-wide (Barlow and Reichard, 2009; Custodio, 2009; Custodio and Bruggeman, 1987). The dimensional analysis in this study is comparable to the problem that was described by Eeman et al. (2011). Therefore, many identical dimensionless groups arise. A difference compared to the analysis of Eeman et al. (2011) is the boundary condition in the intertidal area. An intertidal area with a constant slope introduces three additional dimensionless parameters: α, A_L and f_{ps}. The derivation of these parameters is given in the appendix. Three parameters were chosen from the possible dimensionless parameter groups to define the parameter variations used in the simulations:

- The Rayleigh number R, defined as:

$$R = \frac{\kappa g \Delta\rho_{max}}{\mu N} \tag{5}$$

where κ is the intrinsic permeability [L^2], g is the gravitational acceleration [$L\,T^{-2}$], $\Delta\rho_{max}$ is the maximum density difference of the fluid [$M\,L^{-3}$], μ is the dynamic viscosity [$L\,M^{-1}\,T^{-1}$] and N is the precipitation rate [$L\,T^{-1}$]. In this case, the Rayleigh number can be interpreted as the ratio of the downward force per volume of the fresh water lens (with a given μ of the water and arising from a given κ and N), and the upward, buoyant force on that volume by the saline groundwater.

- The scaled amplitude A_L, defined as:

$$A_L = \frac{L}{A} \tag{6}$$

where A is the tidal amplitude [L] and L is the width of the freshwater lens in vertical cross section [L].

- The slope of the intertidal area α:

$$\alpha = \frac{2A}{B} \tag{7}$$

where B is the width of the intertidal area [L].

R was analyzed because this group has a significant effect on both the lens thickness and the hydraulic heads (Eeman et al., 2011). To vary this group, only the recharge rate N and the fresh water hydraulic conductivity K, which is here defined as $\frac{\kappa g \rho_f}{\mu}$, were varied. For convenience R is expressed in this paper as $10^{-3}\frac{K\Delta\rho_{max}}{N}$ For the remaining part of the paper, the fresh water hydraulic conductivity is simply denoted as 'hydraulic conductivity'. Variations in A_L and α were chosen because they characterize the intertidal area. f_{ps} contains the frequency of the tidal oscillation, the effective porosity, the width of the fresh water lens and the precipitation rate. This group was not considered explicitly, but varies upon variation of A_L and R. For the parameters N, K, L, A and α, a reference value and variations were chosen (Table 1). For α, only the width of the intertidal area B was varied, as A also appears in A_L. The range of α represents intermediate to dissipative intertidal area profiles (Reis and Gama, 2010; Wright and Short, 1984).

For the analytical solution, the time-averaged hydraulic head at the high tide mark from the corresponding numerical model functions as a boundary condition. The analytical solution is based on the solution of van Dam (1983), who assumed mean sea level at the offshore boundary. The derivation of the analytical solution is based upon three governing equations to describe steady state flow in an unconfined coastal aquifer (Fig. 4):

Darcy's law and the Dupuit assumption:

$$q = -K(H+h)\frac{dh}{dx} \tag{8}$$

the continuity equation:

$$dq = Ndx \tag{9}$$

and the Badon Ghijben–Herzberg relationship:

$$h = \delta H \tag{10}$$

where q is the volumetric discharge per unit width of the aquifer [$L^2\,T^{-1}$], H is the depth of the sharp saline-fresh groundwater interface (absolute, and referenced from msl/x-axis) [L], x is the horizontal coordinate (origin at the boundary between regions P and L (Fig. 3a)) [L], h is the hydraulic head (0 in case of msl) [L] and δ is the relative density difference $\left(\frac{\rho_s - \rho_f}{\rho_f}\right)$. Combining Eqs. (8)–(10) and integration yields, after rewriting, the following equation to compute the hydraulic head at location x:

$$h(x) = \delta\sqrt{\frac{-Nx^2 - 2C_1 x}{K\delta(1+\delta)}} \tag{11}$$

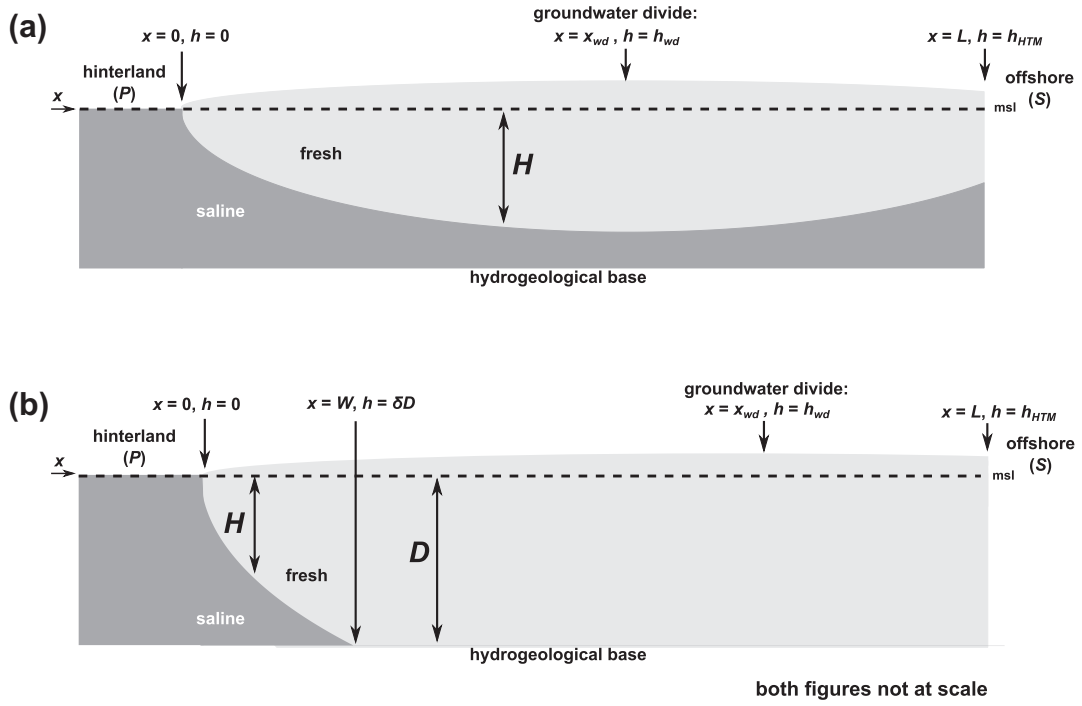

Fig. 4. (a) Freshwater lens in a deep aquifer. x_{wd} is the horizontal location of the groundwater divide, h_{wd} is the hydraulic head of the groundwater divide. (b) Freshwater lens in the shallow aquifer. D is the thickness of the aquifer, relative to mean sea level.

with C_1:

$$C_1 = \frac{\left(\frac{h_{HTM}}{\delta}\right)^2(\delta K + \delta^2 K) + NL^2}{-2L} \tag{12}$$

The location of the groundwater divide can be found by taking the derivative of Eq. (11) with respect to x. Note that L in the time-averaged sea level model is related to L in the corresponding analytical model by $L(\text{numerical}) = L(\text{analytical}) + 0.5B$, as the mean sea level elevation is located in the middle of the intertidal area.

2.5. Fresh water lens in the shallow aquifer

The aquifer is underlain by an impermeable layer at −20 m msl (Fig. 4). The variation of the parameters is shown in Table 2, including the different controlled water levels in the region P.

For the analytical model of the shallow aquifer, the equation for solving the hydraulic head in the region $0 \leqslant x \leqslant W$ is given as:

$$h(x) = \delta\sqrt{\frac{-Nx^2 + 2Nx_{wd}x}{k(1+\delta)\delta}} \tag{13}$$

At $x = W$ (the location of the salt water wedge), H is equal to the depth of the aquifer D (absolute, and referenced from msl/x-axis), so:

Table 2
Parameters used in the case of the fresh water lens in the shallow aquifer.

Dimensionless group	Parameter values	Group value
R (ref)	K = 10 m d^{-1}, N = 0.001 m d^{-1}	250
α	A = 1 m, B = 25 m	0.08
α (ref)	A = 1 m, B = 50 m	0.04
α	A = 1 m, B = 100 m	0.02
A_L	L = 1000 m, A = 0.5 m	2000
A_L (ref)	L = 1000 m, A = 1.0 m	1000
A_L	L = 1000 m, A = 2.0 m	500

$$D^2(x = W) = \frac{-NW^2 + 2Nx_{wd}W}{k(1+\delta)\delta} \tag{14}$$

W can be found by finding the roots of this equation.

For the region $W \leqslant x \leqslant L$, a general equation to describe flow in a shallow unconfined aquifer using the Dupuit assumption was used (Bear, 1972):

$$h(x) = \sqrt{(D+\delta D)^2 - \frac{(D+\delta D)^2 - (h_{HTM}+D)^2}{L-W}(x-W) + \frac{N}{K}((L-x)(x-W))} - D \tag{15}$$

Eqs. (13)–(15) were solved iteratively by adjusting x_{wd}, until h_{wd} is equal in Eqs. (13) and (15).

This analytical solution applies for the cases where $\frac{h_{HTM}}{\delta} \geqslant D$. An analytical solution for a salt water wedge (cf. Eqs. (13) and (14)) in case $\frac{h_{HTM}}{\delta} < D$ resulted in a large difference with the numerical model regarding the location and hydraulic head of the groundwater divide. This can be attributed to the presence of the upper saline plume, which significantly reduces the length of the salt water wedge, as was shown by Kuan et al. (2012).

For the three cases with a different hydraulic head in the region P (h_P), the following equation for the hydraulic head in the region $0 \leqslant x \leqslant L$ (cf. Bear (1972)) was used:

$$h(x) = \sqrt{(D+h_P)^2 - \frac{(D+h_P)^2 - (h_{HTM}+D)^2}{L}x + \frac{N}{K}(L-x)x} - D \tag{16}$$

Note that it is assumed here that $\delta D \leqslant h_P$.

2.6. Fresh water lens in the heterogeneous subsurface

For the analysis of a fresh water lens in the heterogeneous subsurface, a cross sectional model was constructed of a field situation in the Netherlands. The model was calibrated using borehole logs,

hydraulic head data, ground time-domain electromagnetic soundings, a smooth inversion model of an airborne electromagnetic (AEM) survey (for comparable examples see Faneca Sànchez et al. (2012); Viezzoli et al. (2010)), and pressure transducer data in the intertidal area. For further details, we refer to Pauw et al. (2009). Fig. 5 shows the boundary conditions and the distribution of the hydrogeological units that were used to model the heterogeneous distribution of the hydraulic conductivity. In the intertidal area B, the time-averaged hydraulic heads are based on pressure transducer data. At the high tide mark, the time-averaged hydraulic head amounts 0.4 above msl. The length of the intertidal area is approximately 50 m.

3. Results and discussion

3.1. Validation of the step-wise approach

For the validation of the step-wise approach a relatively small model domain was used. The hydrogeological base of the aquifer is located at 10 m below mean sea level, the fresh water lens is 1000 m wide, the tidal amplitude is 1.0 m, the recharge rate is 0.001 m d^{-1}, the isotropic hydraulic conductivity is 10 m d^{-1} and the slope of the intertidal area is 0.02. For the step-wise validation model, the change of the hydraulic head at $x = 0.5L$ as a function of time is shown in Fig. 6. The hydraulic head at $x = 0.5L$ increases rapidly in the first three years. Hereafter, the increase attenuates and stabilizes after approximately 20 years. A small depression is present between 3 and 5 year of simulation time, which can be attributed to the development of the upper saline plume in the intertidal area. In the constant mean sea level model, this depression is absent because there is no tidal forcing. The hydraulic head at $x = 0.5L$ at the end of constant mean sea level model is lower than the hydraulic head at $x = 0.5L$ at the end of the step-wise validation model, viz. the overheight at location $x = 0.5L$ is 0.28 m.

In the periodic sea level model, the hydraulic head at $x = 0.5L$ increases in the course of one year. It must be noted here, that the time-averaged hydraulic head at the high tide mark reached a stable value already after approximately 0.3 year. However, as the time to reach a constant time-averaged hydraulic head at the high tide mark cannot be determined a priori, the simulation time of the periodic sea level model is longer. The time-averaged sea level model shows that the hydraulic head at $x = 0.5L$ increases slightly during two years, after which it reaches a stable value. The overheight at $x = 0.5L$, calculated from the difference between the constant mean sea level model and the time-averaged mean sea level model, equals 0.28 m. This corresponds to the overheight calculated from the step-wise validation model. It should be noted here that this correspondence in overheight not only holds for $x = 0.5L$, but along the total width L of the fresh water lens. This example shows that the step-wise approach is appropriate to investigate the regional scale overheight.

Fig. 7 suggests that there is also a reasonable correspondence in the groundwater salinity distribution between the step-wise validation model and the time-averaged sea level model. For this set of parameters though, the upper saline plume does not have a stable shape. Due to the observed fingering patterns and the unstable density distribution, the unstable shape of the upper saline plume is explained here by free convection processes. Free convection in the upper saline plume was also present in some of the other simulations. However, it is beyond the scope of this paper to investigate the parameters that govern free convection in the intertidal area.

3.2. Fresh water lens in the deep aquifer

Fig. 8 depicts the time-averaged hydraulic head at the high tide mark for the combinations of dimensionless groups. The response of the overheight at the high tide mark upon a change of the dimensionless groups is in line with what can be expected qualitatively from previous investigations (e.g., Lebbe (1983); Nielsen (1990); Turner et al. (1995)). An increase of the Rayleigh number R results in a smaller overheight at the high tide mark because a more permeable intertidal area is easier to drain than a less permeable one. An increase of the slope of the intertidal area α results in faster drainage of the intertidal area, so the overheight therefore decreases. As the Scaled Amplitude A_L increases, more water infiltrates in the intertidal area due to an increase of the tidal amplitude, so the overheight increases. The sensitivity of α and A_L, indicated by the slope of the lines in Fig. 8, increases with a decrease of R. Hence, for a less permeable intertidal area, changes in the slope of the intertidal area and in the tidal amplitude are more outspoken compared to a more permeable intertidal area.

Fig. 8 suggests an approximately linear relationship between the time-averaged hydraulic head at the high tide mark and the log-transformed values of the three dimensionless groups. For the dominant parameters of the groundwater flow in the intertidal area (K (m/d), A (m) and α), a linear equation was fitted to estimate the time-averaged hydraulic head at the high tide mark (in m):

$$h_{HTM} = c_1 + c_2 \log A + c_3 \log \alpha + c4 \log A \log \alpha \quad (17)$$

with $c_1 = -0.332 \log K + 0.652$, $c_2 = -1.744 \log K + 3.519$, $c_3 = 0.083 \log K - 0.368$ and $c_4 = 0.033 \log K - 0.140$.

Note that this equation implicitly assumes that the influence of L and N on h_{HTM} is negligible for the parameter range that is considered here. In other words, the flow of fresh groundwater from the hinterland to the sea does not have a significant influence on the decrease of the hydraulic heads in the intertidal area during falling

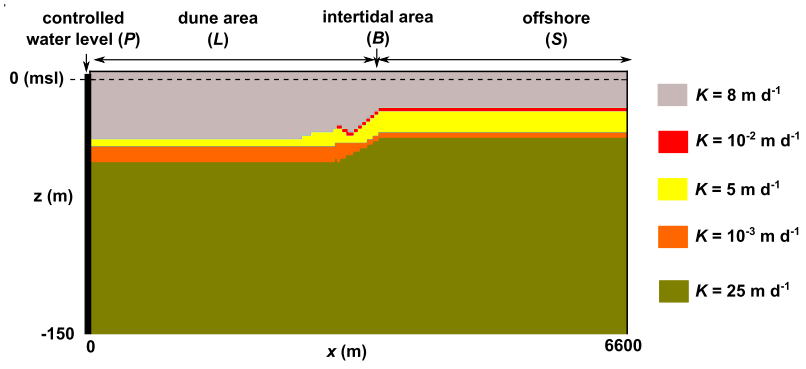

Fig. 5. Overview of the boundary conditions and distribution of hydrogeological units of the model of the freshwater lens in the heterogeneous subsurface. The right and bottom boundaries are no-flow boundaries. The left boundary (the hinterland P) is a constant head and constant concentration boundary. The isotropic hydraulic conductivity values are displayed at the right. Note that B is a region (intertidal area), but that for scaling reasons it is indicated here with a single arrow.

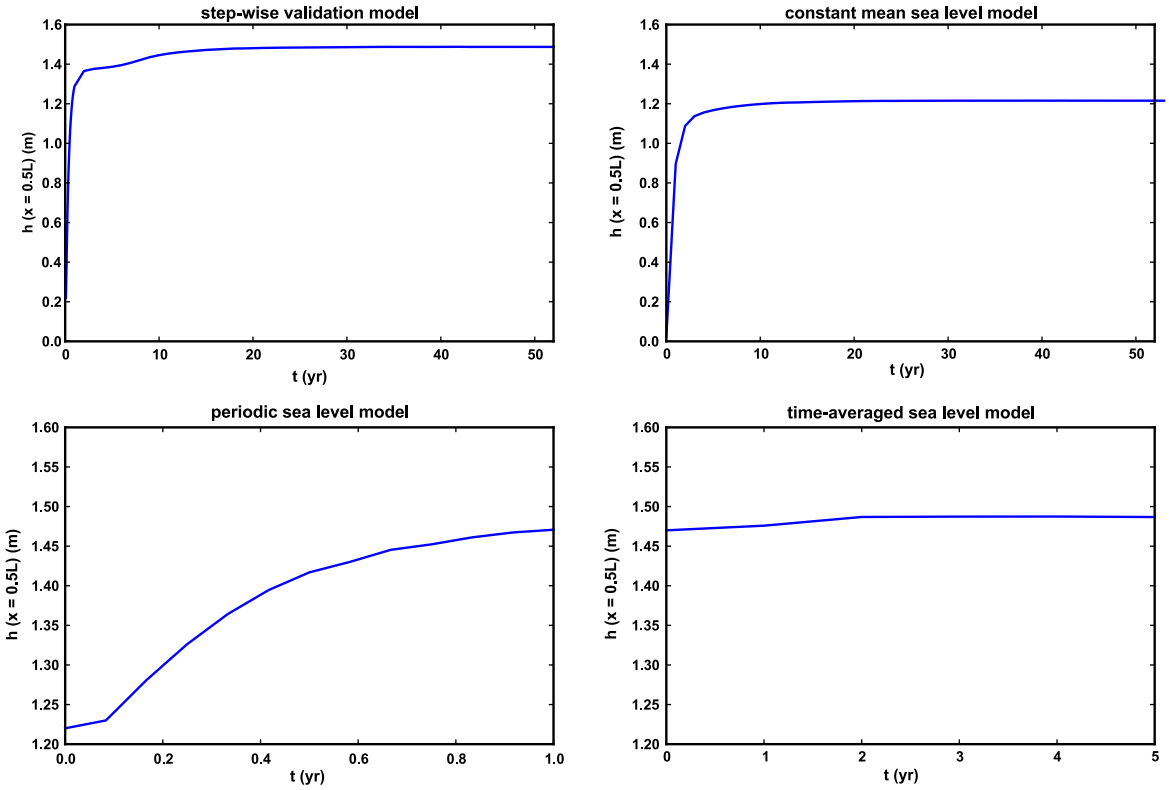

Fig. 6. The change of the hydraulic head at $x = 0.5L$ for the step-wise validation model, mean sea level model, periodic sea level model and time-averaged sea level model. Note that the upper and lower subfigures have different horizontal and vertical scales.

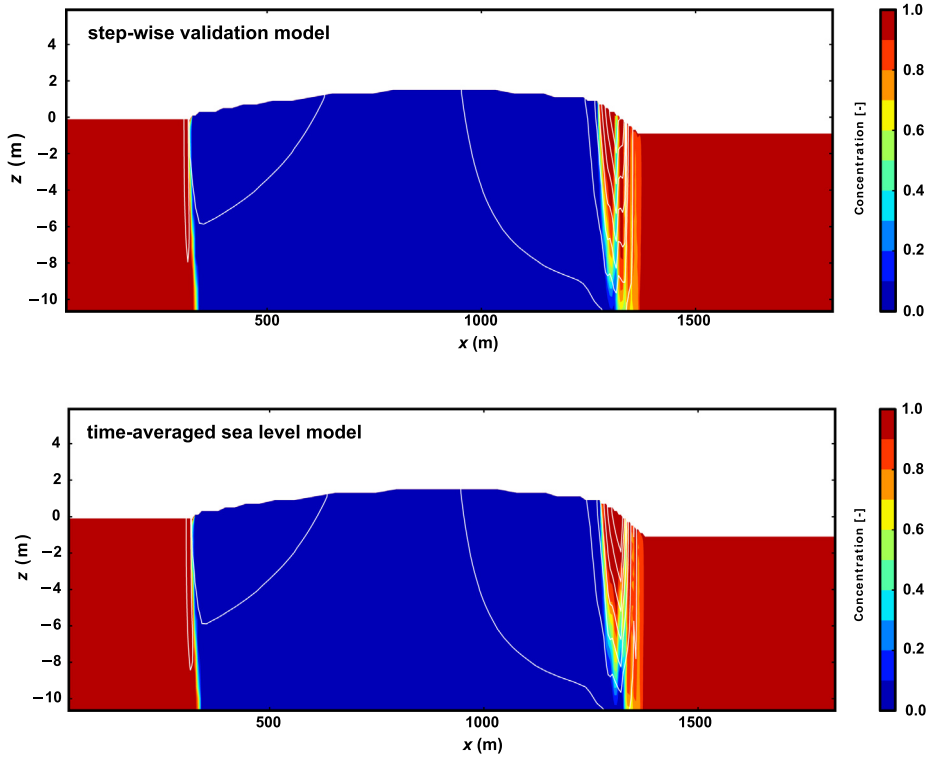

Fig. 7. The groundwater salinity distribution and streamlines (in white) of the step-wise validation model and the time-averaged sea level model.

tide (again, for the considered parameter range). The root mean square (RMS) error of this relationship is 0.09 m, which indicates that the assumption is reasonable. The error especially increases when the width of the fresh water lens is large compared to the width of the intertidal area (i.e., for high values of A_L). In these cases, h_{HTM} is underestimated, so the influence of the offshore directed flow of fresh water has some influence. Fortunately, as will be explained further, the influence on the regional scale

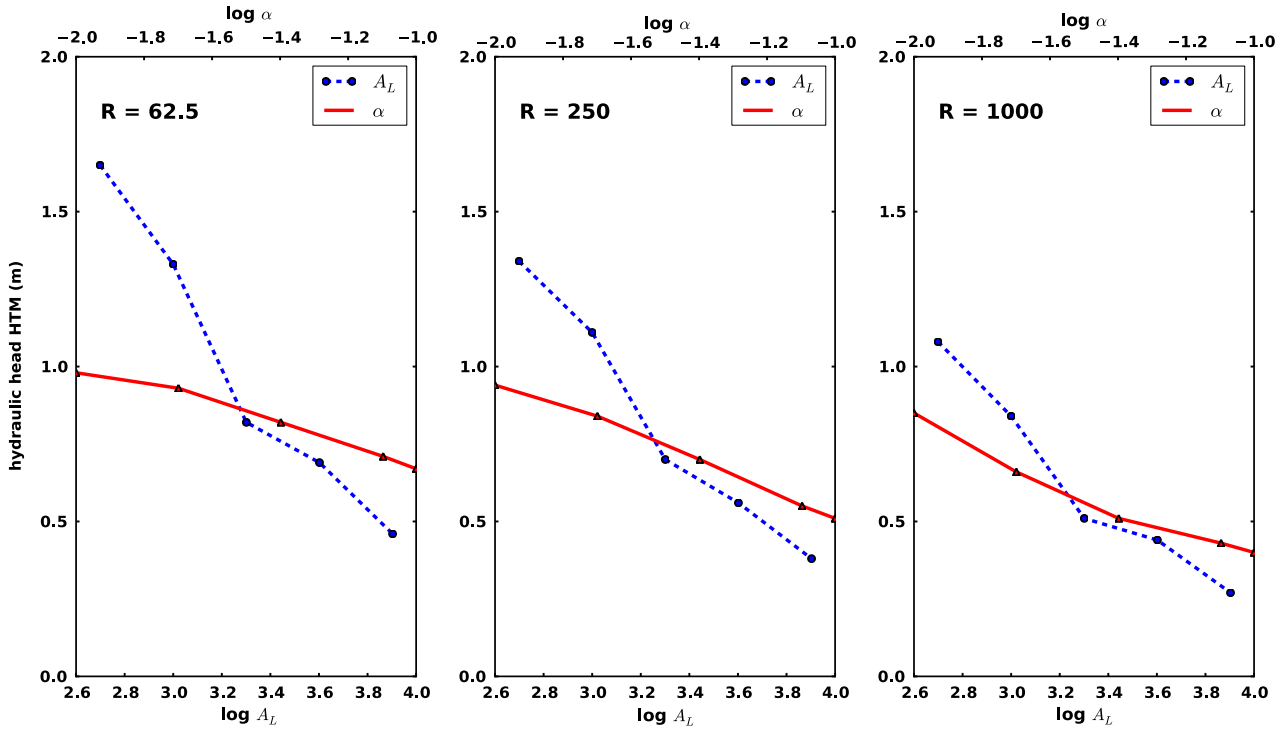

Fig. 8. Time-averaged head at the high tide mark (HTM) for all the combinations of dimensionless groups for the fresh water lens in a thick aquifer.

overheight is in these cases low. If the three largest values of A_L are taken out of the RMS calculation, the RMS decreases to 0.08 m and all values for h_{HTM} can be estimated within 0.1 m.

Fig. 9 shows the relative hydraulic head change at $x = 0.5L$, for the dimensionless groups A_L and α. The relative hydraulic head change $\Delta h'$ is used as a measure for the (relative) overheight:

$$\Delta h' = \left(\frac{h_{TASL}}{h_{CMSL}} - 1\right) \tag{18}$$

where h_{TASL} is the hydraulic head in the time-averaged sea level model and h_{CMSL} is the hydraulic head in the constant mean sea level model, both at $x = 0.5L$. The rationale of defining a relative overheight is related to scaling; the absolute 'error' (i.e., the underestimated hydraulic head) that is introduced in a model if tidal forcing is neglected becomes less 'important' when the scale of the problem (and hence, the hydraulic head) increases. The absolute error can be estimated using the hydraulic head at $x = 0.5L$ from the corresponding analytical solution. According to the analytical solution, the hydraulic head at $x = 0.5L$ is equal to 1.56 m. Fig. 9 shows that $\Delta h'$ is approximately 4%. Hence, the hydraulic head at $x = 0.5L$ in the simulation where tidal forcing is taken into account is 1.62 m.

Fig. 9 shows that $\Delta h'$ increases with increasing values of R. This behavior is different from the influence of R on the overheight at the high tide mark. The influence of the overheight at the high tide mark is larger when the hydraulic head at the groundwater divide is relatively low. As a decrease of A_L and α results in a larger overheight at the high tide mark, the influence also increases for $\Delta h'$. The sensitivity of A_L is larger than α, similar as was observed for the influence on the overheight at the high tide mark.

Fig. 10 shows the effect of the dimensionless groups on the relative change of the groundwater divide $\Delta x'$ (analogous to the relative overheight), which was computed with:

$$\Delta x' = \frac{x_{wd-TASL} - x_{wd-CMSL}}{0.5L} \tag{19}$$

where $x_{wd-TASL}$ is the location of the groundwater divide in the time-averaged sea level model and $x_{wd-CMSL}$ is the location of the groundwater divide in the constant mean sea level model. As expected, the effects of the dimensionless groups on the relative change of the groundwater divide are comparable to the effect on the relative overheight $\Delta h'$. The results of $\Delta x'$ indicate how the distribution of fluxes to the hinterland and the sea change, when tidal forcing is taken into account.

Table 3 shows the results of the comparison between the time-averaged sea level model and the corresponding analytical solution. The relative difference in hydraulic head at $x = 0.5L$ ($\Delta h'_{(num-ana)}$) is computed as:

$$\Delta h'_{(num-ana)} = \frac{h_{num} - h_{ana}}{h_{num}} \tag{20}$$

where h_{num} is the hydraulic head at location $x = 0.5L$ in the time-averaged sea level model and h_{ana} is the hydraulic head at location $x = 0.5L$ in the corresponding analytical solution. The relative difference in location of the groundwater divide between these models $\Delta x'_{(num-ana)}$ is computed with:

$$\Delta x'_{(num-ana)} = \frac{x_{num} - x_{ana}}{0.5L} \tag{21}$$

where x_{num} is the location of the groundwater divide in the time-averaged sea level model and x_{ana} is the location of the groundwater divide in the corresponding analytical solution. h_{num} and x_{num} are computed using interpolation of the two nodes of maximum hydraulic head. The estimated error due to this interpolation is in the order of 0.01 m for h_{num} and 5 m for x_{num}.

$\Delta x'_{(num-ana)}$ and $\Delta h'_{(num-ana)}$ generally increase with increasing values of R, and decreasing values of α and A_L. When the time-averaged head at the high tide mark is high compared to the hydraulic head at the groundwater divide, the analytical model is less accurate. Negative values of $\Delta x'_{(num-ana)}$ indicate that the computed change of the groundwater divide in the analytical equation is higher compared to the one computed with the numerical model.

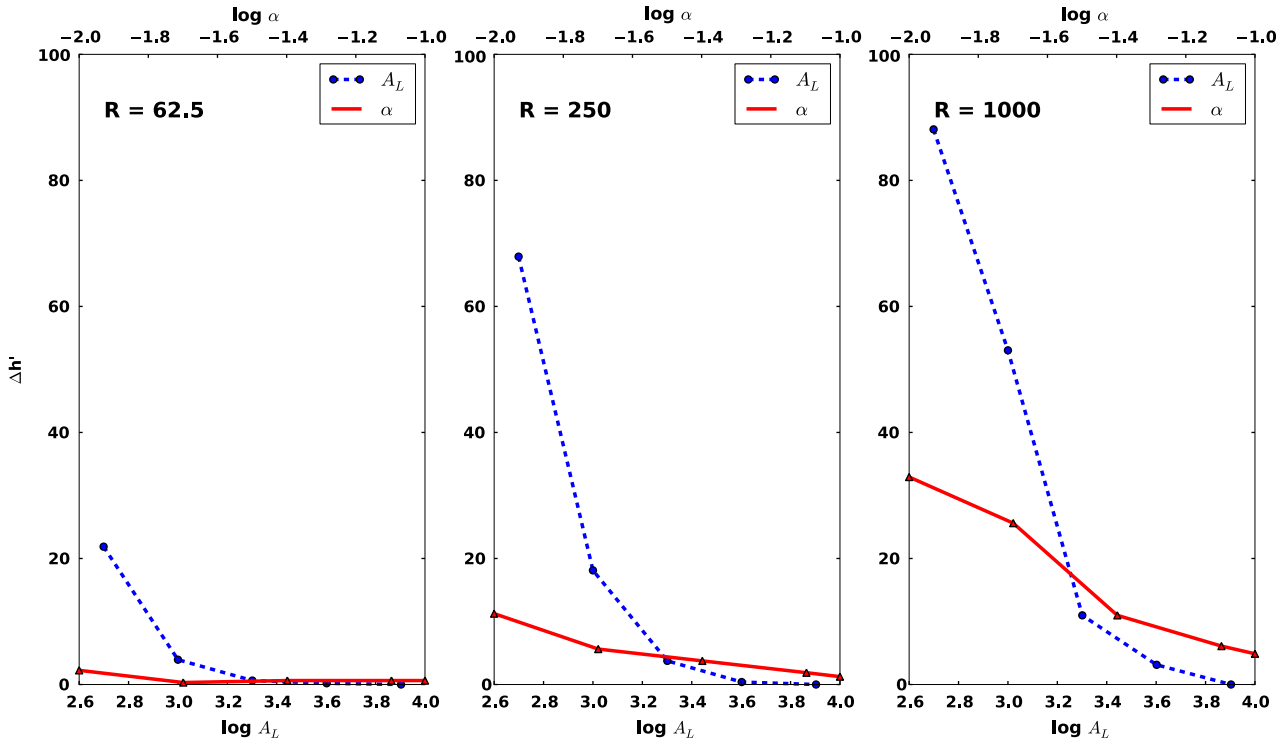

Fig. 9. Relative change of the hydraulic head ($\Delta h'$) at $x = 0.5L$ for the combinations of the dimensionless groups R, A_L and α.

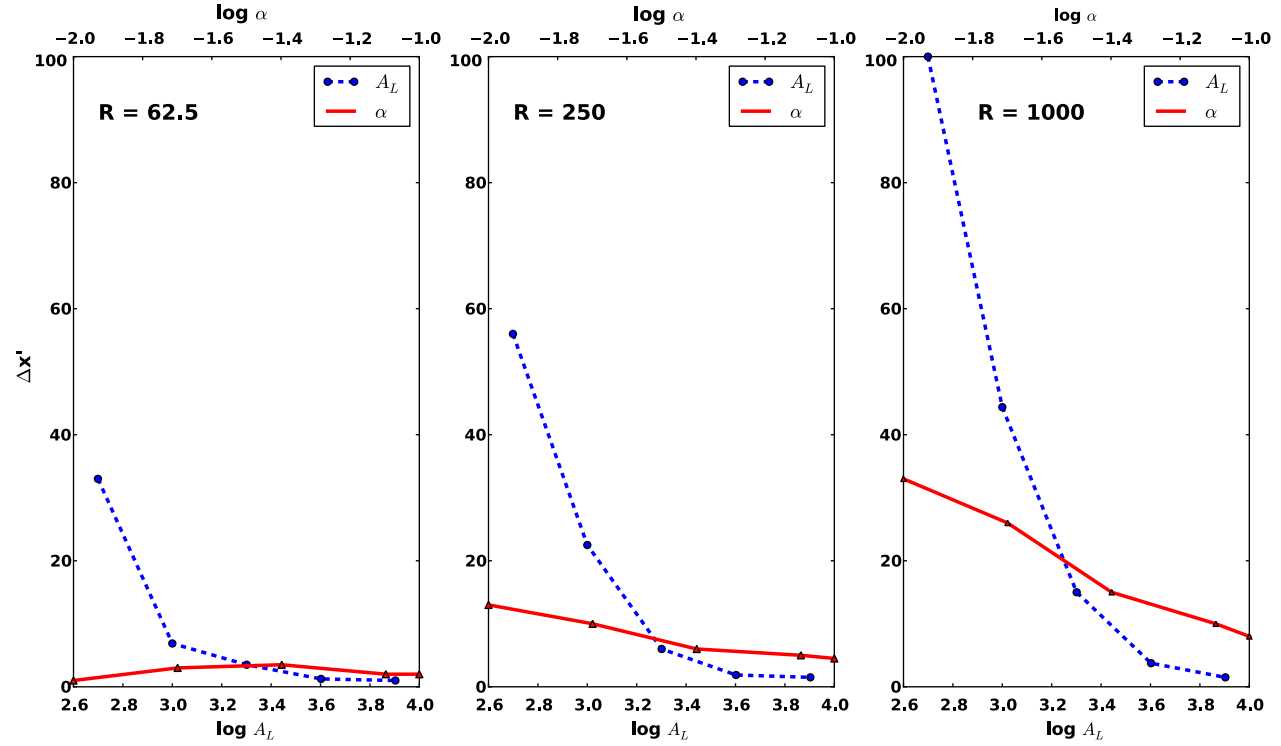

Fig. 10. Relative change of the location of the groundwater divide ($\Delta x'$) for the combinations of the dimensionless groups R, A_L and α.

3.3. Fresh water lens in the shallow aquifer

Fig. 11 shows $\Delta x'$ and $\Delta h'$ for the dimensionless groups that were considered for the fresh water lens in the shallow aquifer. Similar to what was observed for the fresh water lens in the deep aquifer is that A_L is more sensitive than α. Although different values of R were not considered for the fresh water lens in the shallow aquifer, a similar behavior can be expected as was described for the fresh water lens in the deep aquifer. Comparing the results of a deep and shallow aquifer for $A_L = 500$, 1000 and 2000 with $R = 250$ and $\alpha = 0.04$, reveals that although the absolute overheight at the high tide mark is larger in the shallow aquifer (Nielsen,

Table 3
$\Delta h'_{(num-an)}$ and $\Delta x'_{wd(num-an)}$ for the combinations of dimensionless groups in the analysis of a fresh water lens in a thick aquifer.

Dimensionless group	Group value	$\Delta h'_{(num-an)}$	$\Delta x'_{wd(num-an)}$
$R = 62.5$			
α	0.01	1.9	−1.5
α	0.02	1.6	0.8
α	0.08	1.9	0.8
α	0.10	2.2	0.9
A_L	500	1.5	4.5
A_L	1000	0.4	−0.3
A_L	2000	1.9	1.8
A_L	4000	1.2	0.8
A_L	8000	1.3	0.9
$R = 250$			
α	0.01	8.4	3.6
α	0.02	3.6	2.7
α	0.08	1.8	2.0
α	0.10	1.9	1.9
A_L	500	10.3	−19.4
A_L	1000	2.7	2.5
A_L	2000	2.4	1.0
A_L	4000	1.6	0.6
A_L	8000	1.3	1.2
$R = 1000$			
α	0.01	12.8	1.9
α	0.02	13.6	7.8
α	0.08	4.6	2.5
α	0.10	4.7	1.5
A_L	500	−7.6	2.8
A_L	1000	14.9	−1.5
A_L	2000	6.6	4.3
A_L	4000	3.0	0.6
A_L	8000	2.5	0.8

1990), $\Delta h'$ and $\Delta x'$ differ no more than 5%. This is because the reduced thickness of the aquifer not only increases the overheight at the high tide mark, but also increases the hydraulic head at the groundwater divide, so that the influence of the overheight at the high tide mark on the relative regional scale overheight decreases. The difference in h_{HTM} between the cases of the deep and the shallow aquifer is within 0.05 m, except for A_L, for which it is 0.21 m.

In the simulations with a higher water level in the region P, $\Delta h'$ was computed using the hydraulic head at the groundwater divide in the mean sea level model, because the groundwater head was not located at $x = 0.5L$. The values of $\Delta h'$ for the hydraulic head at the region P of 0.5 m, 1.0 m and 1.5 m are 18%, 10% and 5%, respectively. Hence, $\Delta h'$ increases as the hydraulic head in the region P decreases, just like what was observed for the previous cases. Not surprisingly, $\Delta x'$ behaves similarly.

The differences between the numerical and the corresponding analytical solutions considering the relative difference in hydraulic head at location $x = 0.5L$, are minor (Table 4). The absolute difference in hydraulic head at location $x = 0.5L$ is within 0.1 m for all combinations of dimensionless groups. The difference regarding the location of the groundwater divide is somewhat larger, but the relative difference is $\leqslant$10%. The relative difference of the groundwater divide for the cases where $P >$ msl was not considered, because the location of the groundwater divide could not be referenced to $0.5L$. Note that for the dimensionless group $A_L = 1000$ the analytical solution could not be computed since $\frac{h_{HTM}}{\delta} < D$.

3.4. Fresh water lens in the heterogeneous subsurface

For the fresh water lens in the heterogeneous subsurface, the time-averaged sea level model and the constant mean sea level model indicate that the regional scale overheight is minor; the difference in the computed groundwater divide is 42 m and the difference in hydraulic head is 0.01 m. Not surprisingly, the groundwater salinity distribution is also comparable. Fig. 12 shows the simulated groundwater salinity distribution and the inversion model of the airborne electromagnetic (AEM) data. The 10 Ωm contour in the AEM model served as calibration for the position of the deep groundwater salinity transition zone in the numerical model. It should be noted here that this case only serves as an illustration of how to apply the findings of the previously discussed, synthetic cases to a real world case which is less idealized.

As the subsurface is heterogeneous, the analytical solutions that were derived for the shallow and the thick aquifer cannot be used directly. However, the analytical solution for the thick aquifer is used as an estimate. The harmonic average of the hydraulic conductivity and aquifer thickness of the first, second, and third aquifer is used to determine K at 13 m d^{-1}. $A = \sim 0.8$ and $\alpha = 0.04$ because $\sim B = 50$ m. From Eq. (17) the time-averaged head at high tide mark is estimated around 0.5 m. This is 0.1 m higher than the head that was measured with pressure transducer data, which can be explained by the higher hydraulic conductivity of the intertidal sediments compared to the hydraulic conductivity of the aquifer (Pauw et al., 2009). Using Eq. (11), the absolute head at location $x = 0.5L$ is determined at 2.76 m msl. This is much lower than in the numerical model (4.7 m msl), and can be explained by the presence of a semi-permeable layer and the high hydraulic head that at the boundary P. The analytical solution indicates that the influence of the overheight is minor; the shift of the groundwater divide is 16 m, whereas there is essentially no difference in head at location $x = 0.5L$. This estimate is within the error range of the analytical solution. Moreover, if R is increased by adjusting K to 4.5 m d^{-1}, such that hydraulic head increases according to the measured value, the analytical solution indicates an even smaller influence on the groundwater divide.

4. Discussion

To date, the numerical modeling of density dependent groundwater flow and salt transport in regional scale coastal aquifers is still strongly limited by computation time constraints (Post, 2005; Werner et al., 2013). Many studies have been devoted to circumvent this problem. Examples are vertical averaging of the governing equations (Pool et al., 2011) and sharp interface modeling (Bakker, 2003; Essaid, 1986). For the same reason, tides are rarely taken into account in modeling studies of regional scale groundwater flow in coastal aquifers. Instead, the boundary condition at the land-sea boundary is often based on a constant mean sea level. In this paper, the validation example of the stepwise approach nicely illustrates such a difference in computation time; on a 3 GHz desktop computer, the simulation of the model with only periodic sea level variation took approximately 6.5 days, whereas the three models in the step-wise approach together took about 8 h. The implications for three-dimensional modeling are evident.

The results in this paper show that tidal forcing should, under certain conditions, be accounted for in regional scale coastal aquifer studies. Quantitative guidance is provided here to estimate the effects of tidal forcing on the time-averaged hydraulic head at the high tide mark, and the hydraulic head and location of the groundwater divide. Important assumptions that were made are a constant (both in space and time) slope of the intertidal area, a diurnal tidal cycle without changes in tidal amplitude, no effects of waves and storms, a constant and equally distributed groundwater recharge and a homogeneous and isotropic porous medium. In addition, the influence of phreatic storage on the overheight was not considered. These complications may be the subject of further investigations, in particular, the effect of wave runup on the time-averaged hydraulic

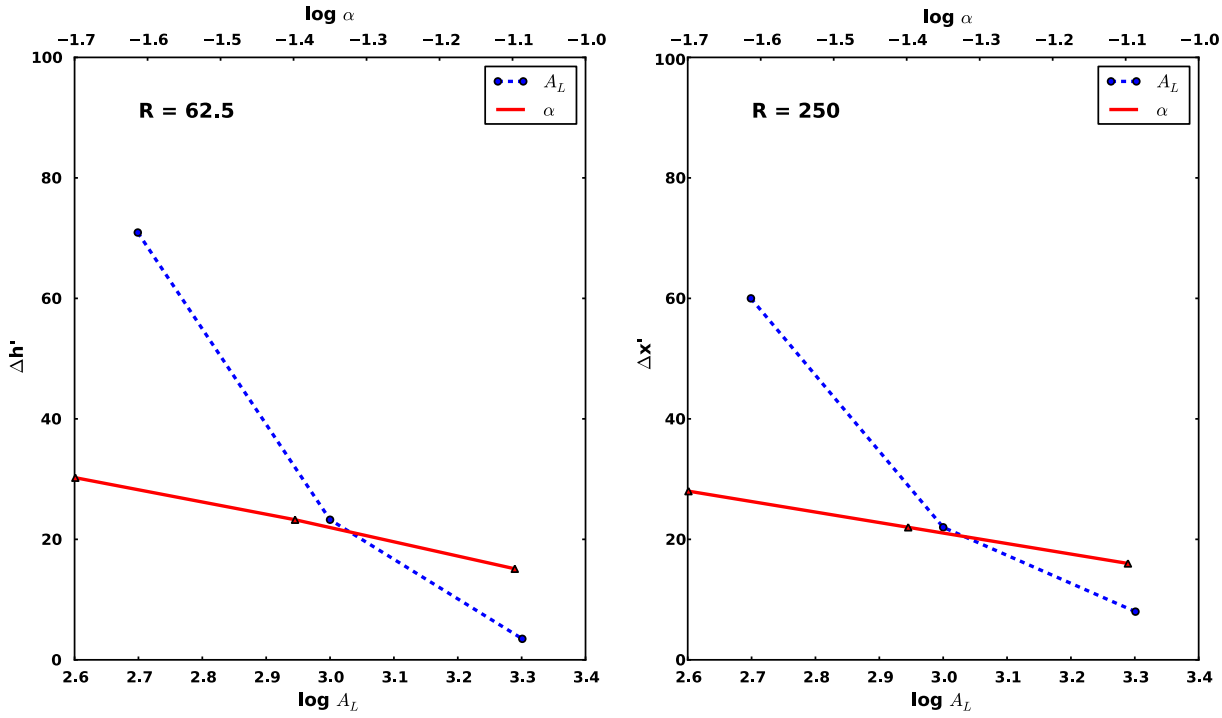

Fig. 11. Results of the numerical simulations of the fresh water lens in the shallow aquifer.

Table 4
$\Delta h'_{(num-ana)}$ and $\Delta x'_{(num-ana)}$ for the considered combination of dimensionless groups in the analysis of the fresh water lens in the shallow aquifer.

Dimensionless group	Group value	$\Delta h'_{wd(num-ana)}$	$\Delta x'_{wd(num-ana)}$
α	0.08	1	6
α	0.02	2	7
A_L	2000	–	–
A_L	1000	2	6
A_L	500	1	7
A_L ($P = 0.5$)	1000	1	–
A_L ($P = 1.5$)	1000	3	–
A_L ($P = 2.0$)	1000	1	–

head at the high tide mark. In a comparison of water table time series from a wave-exposed site and an unexposed site of the Palm Beach Isthmus (Australia), Nielsen (1999) showed that the contribution of waves on the time-averaged hydraulic head in the nearshore region was significantly larger than the contribution of tides. Despite the potential contribution of wave runup, a detailed analysis on its influence on the time-averaged hydraulic head in the nearshore region for different hydrogeological conditions is beyond the scope of this work. The results of this paper should be considered as a conservative estimate of the overheight, especially when there is frequent wave action and the wave height is equal to or larger than the tidal amplitude.

The emphasis of this study is on the regional scale impact of tidal forcing. For local scale studies (Li et al., 2009; Robinson et al., 2007; Xin et al., 2010) the results are less relevant because the computation time is a smaller problem. In addition, in local scale studies the explicit modeling of tides is often needed to capture the governing processes of the problem at hand. Nevertheless, the results in this paper can be used to determine the boundary conditions in the local scale model, such as the amount of fresh groundwater that flows from the groundwater divide to the intertidal area.

The analytical studies by Nielsen (1990) and Teo et al. (2003) have previously addressed the effect of tidal forcing on unconfined aquifers. The results in this paper are complementary to the results presented in those studies, because here density dependent groundwater flow, salt transport, a seepage face, precipitation excess in the hinterland and other different hydrogeological conditions are considered. A comparison between the results in this paper and the results of Teo et al. (2003), which can be considered as an extension of the work by Nielsen (1990), is not straightforward. The difficulty is due to the validity of the analytical solutions of Teo et al. (2003). Their solutions are valid for small values of the shallow water parameter ϵ and the amplitude parameter α:

$$\epsilon = \sqrt{\frac{D\omega n_e}{2K}} \tag{22}$$

and

$$\alpha = \frac{A}{D} \tag{23}$$

where D is the still water table height, ω is the tidal wave frequency, n_e is the porosity, K is the hydraulic conductivity of the aquifer and A is the tidal amplitude. For the hydrogeological conditions that are considered in this paper, D is often hard to determine and, more important, ϵ is not much smaller than 1. In fact, most parameter combinations result in values of ϵ around 1, which is representative for dissipative beaches.

Nielsen (1990) already indicated that the analytical solution yields large discrepancies with field observations when a seepage face is present in the intertidal area. Comparison with field data showed an underestimation of the hydraulic heads by the analytical solution of up to 0.3 m, for a (small) tidal amplitude of 0.5 m and a (large) beach slope of 0.06. Because the overheight increases when the tidal amplitude increases and beach slope decreases, it is advised here that for comparable hydrogeological conditions as the ones considered in this paper, the seepage face should be taken into account.

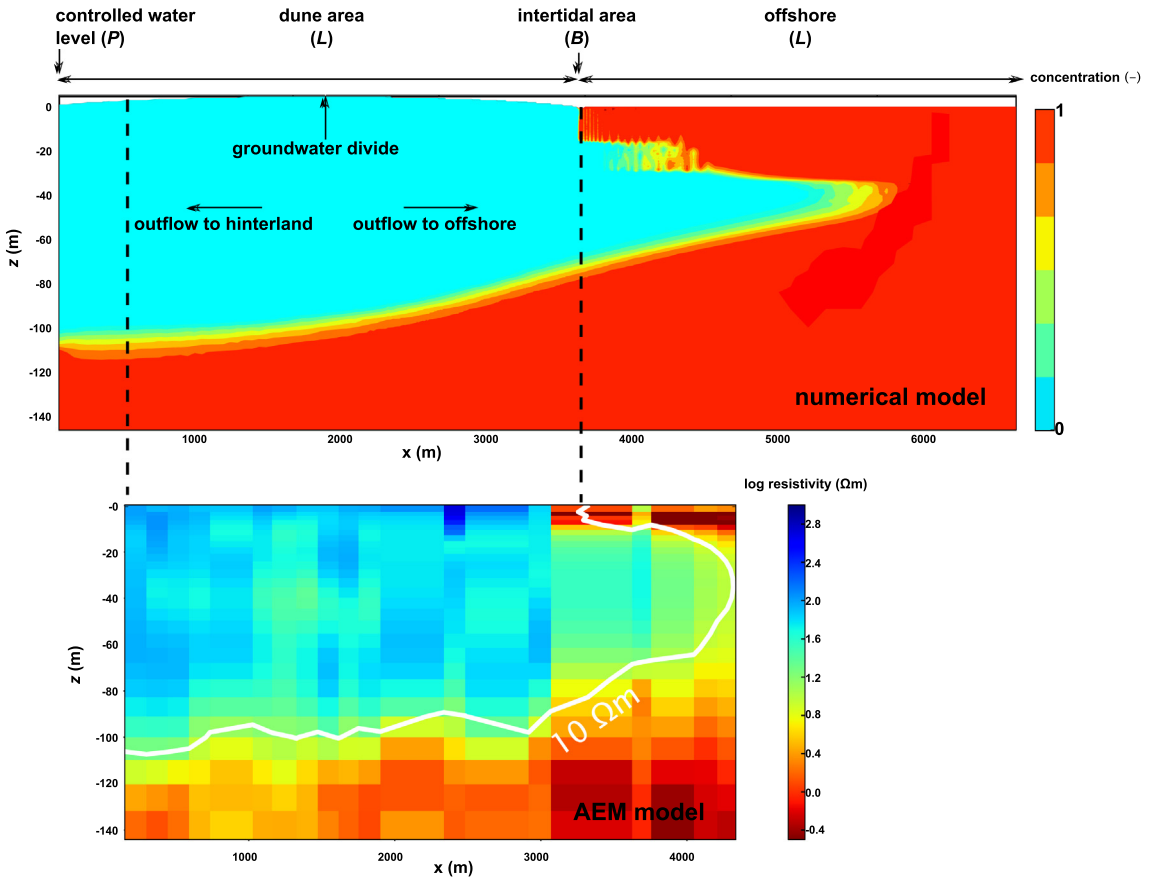

Fig. 12. Results of the numerical simulation of the time-averaged sea level model of a regional scale fresh water lens in a heterogeneous subsurface (above), and the inversion model of AEM survey across this transect (below). Both the AEM model and numerical model indicate the presence of a fresh water tongue below the sea floor.

5. Summary and conclusions

The scope of this paper was to provide a quantitative indication of the bias that is introduced in a groundwater flow model of an unconfined coastal aquifer if tides are neglected. Numerical, variable density groundwater flow models were used to determine this bias for a wide range of hydrogeological conditions. Both a shallow and a deep aquifer were investigated with regard to three dimensionless parameter groups that determine the groundwater flow to a large extent. Analytical expressions were presented that allow for a quick estimate of the regional scale effect of tidal forcing under the same conditions as used in the numerical simulations.

Numerical model results indicate that the time-averaged hydraulic head at the high tide mark increases with a decrease of each of the three considered dimensionless parameter groups: R (including the ratio of the hydraulic conductivity and the precipitation excess), α (the slope of the intertidal area) and A_L (the ratio of the width of the fresh water lens and the tidal amplitude). From the results, an empirical relationship was derived which can be used to estimate the time-averaged hydraulic head at the high tide mark from the slope of the intertidal area, the tidal amplitude and the hydraulic conductivity of the intertidal sediment. The time-averaged hydraulic head is used in an analytical model as a boundary condition.

The relative change of the location and the hydraulic head of the groundwater divide, which are jointly referred to as 'regional scale overheight' and are used to characterize regional groundwater flow, increase as α and A_L decrease, but decrease as R decreases. In case of a shallow aquifer, the time-averaged hydraulic head at the high tide mark is larger compared to a deep aquifer. However, the regional scale overheight is comparable. In case the controlled water level in the hinterland is larger than mean sea level, the regional scale overheight decreases. An additional case of a heterogeneous aquifer system based on a real-world situation was also presented. The results of the idealized cases could be used to estimate the regional scale overheight in a more complex system.

The difference between the numerical results of the deep and shallow aquifer and the corresponding analytical solutions is small. Therefore, the presented analytical solutions can be used to estimate the bias that is introduced in a numerical model if tidal forcing is neglected, for a wide range of hydrogeological conditions. However, one should be aware of the fact that this paper considers tidal forcing only. In case of significant wave action, the results in this paper should be considered as conservative estimates.

Acknowledgments

We thank Peter Nielsen (University of Queensland) for this constructive comments on this work. Python modules of the FloPy Project (http://code.google.com/p/flopy/) were used to pre- and postprocess the numerical models in this study. We thank Michel Groen (VU University Amsterdam) for his remarks on the draft of the paper, and Chris Langevin (USGS) for his suggestions on how to improve the numerical stability in the numerical models. We thank Frans Schaars (Artesia Water), Harry Rolf, Sander de Haas and Igor Mendizabal (PWN water supply company) for the AEM dataset. We thank Theo Olsthoorn (Delft University of Technology) for his suggestion on contouring the streamfunction using the cell-by-cell flux output of SEAWAT, which improved the understanding

of the numerical model output. This work was carried out within the Dutch 'Knowledge for Climate' program.

Appendix

For the domain $[-A \leqslant z \leqslant A]$, the position x in the intertidal area is defined as:

$$x = \frac{z}{\tan \alpha} \tag{24}$$

with z being the vertical coordinate (elevation relative to mean sea level) and α the slope of the intertidal area. At mean sea level, $z = 0$ and $x = 0$. In dimensionless form, whereby reference values are denoted by a subscript $(_r)$ and dimensionless quantities by ', Eq. (24) becomes:

$$\frac{x_r}{z_r} \tan\ \alpha = \frac{z'}{x'} \tag{25}$$

Choosing x_r and z_r as the already defined reference length L, the dimensionless group $\tan \alpha$ appears.

A pressure $(P_b(x,t))$ $[\mathrm{M\,L^{-1}\,T^{-2}}]$ is prescribed for the surface of the intertidal area, as a function of position x and time t. When the sea level is lower than or equal to the elevation at point x in the intertidal area, P_b equals 0. In this way a seepage face is simulated (Mulligan et al., 2011). When the sea level is higher than the elevation at point x in the intertidal area, the pressure equals:

$$P_b(x,t) = A \sin(2\pi f t)\rho_{max} g - \rho g z(x) \tag{26}$$

where A is the tidal amplitude, f is the frequency, and g is the gravitational acceleration. If z is referenced to tidal amplitude A, both sides are divided by $A\rho_{max}g$ and ρ_{max} is defined as $(\Delta\rho)_{max}$, the Rayleigh number defined by Eeman et al. (2011) appears. After introduction of reference values, the left hand side of Eq. (26) becomes:

$$\frac{P_b}{A_r \rho_{max} g} \tag{27}$$

with P_b being equal to the reference pressure (Eeman et al., 2011):

$$\frac{\mu N L}{k} \tag{28}$$

whereby N is the recharge rate, k is the permeability of the porous medium and μ is the viscosity of freshwater. The left hand side becomes:

$$\frac{\mu N L}{k A_r \Delta\rho_{max} g} \tag{29}$$

which equals:

$$\frac{L}{A_r R} \tag{30}$$

R is the dimensionless Rayleigh number defined by Eeman et al. (2011) and the dimensionless group A_L appears.

If the definition for the reference time by Eeman et al. (2011) is adopted:

$$t_r = \frac{nL}{N} \tag{31}$$

the following dimensionless group appears from right hand side of Eq. (26):

$$f_{ps} = \frac{fLn}{N} \tag{32}$$

References

Ataieashtiani, B., Volker, R., Lockington, D., 1999. Tidal effects on sea water intrusion in unconfined aquifers. J. Hydrol. 216 (1-2), 17–31.

Bakker, M., 2003. A Dupuit formulation for modeling seawater intrusion in regional aquifer systems. Water Resour. Res. 39 (5), 1–10.

Barlow, P.M., Reichard, E.G., 2009. Saltwater intrusion in coastal regions of North America. Hydrogeol. J. 18 (1), 247–260.

Bear, J., 1972. Dynamics of Fluids in Porous Media. Dover Publications, New York.

Cartwright, N., 2004. Groundwater Dynamics and the Salinity Structure in Sandy Beaches. Ph.D. thesis, University of Queensland, Department of Civil Engineering.

Custodio, E., 2009. Coastal aquifers of Europe: an overview. Hydrogeol. J. 18 (1), 269–280.

Custodio, E., Bruggeman, G., 1987. Groundwater Problem in Coastal Areas. In: Studies and Reports in Hydrology. UNESCO, Paris.

Eeman, S., Leijnse, A., Raats, P.A.C., van der Zee, S.E.A.T.M., 2011. Analysis of the thickness of a fresh water lens and of the transition zone between this lens and upwelling saline water. Adv. Water Resour. 34 (2), 291–302.

Eeman, S., van der Zee, S.E.A.T.M., Leijnse, A., de Louw, P.G.B., Maas, C., 2012. Response to recharge variation of thin rainwater lenses and their mixing zone with underlying saline groundwater. Hydrol. Earth Syst. Sci. 16 (10), 3535–3549.

Essaid, H., 1986. A comparison of the coupled fresh water-salt water flow and the Ghyben–Herzberg sharp interface approaches to modeling of transient behavior in coastal aquifer systems. J. Hydrol. 86 (1-2), 169–193.

Faneca Sànchez, M., Gunnink, J.L., van Baaren, E.S., Oude Essink, G.H.P., Siemon, B., Auken, E., Elderhorst, W., de Louw, P.G.B., 2012. Modelling climate change effects on a Dutch coastal groundwater system using airborne electromagnetic measurements. Hydrol. Earth Syst. Sci. 16 (12), 4499–4516.

Gelhar, L.W., Welty, W., Rehfeldt, K., 1992. A critical review of data on field-scale dispersion of aquifers. Water Resour. Res. 28 (4), 1955–1974.

Hill, M.C., 1990. Preconditioned Conjugate-Gradient 2 (PCG), A Computer Program for Solving Ground-Water Flow Equations. US Geological Survey Water-Resources Investigations Report 90-4048.

Horn, D., 2006. Measurements and modelling of beach groundwater flow in the swash-zone: a review. Cont. Shelf Res. 26 (5), 622–652.

Kaleris, V., 2006. Submarine groundwater discharge: effects of hydrogeology and of near shore surface water bodies. J. Hydrol. 325 (1–4), 96–117.

Kang, H.-Y., 1995. Water Table Dynamics Forced by Waves. Ph.D. thesis, University of Queensland, Department of Civil Engineering.

Kuan, W.K., Jin, G., Xin, P., Robinson, C., Gibbes, B., Li, L., 2012. Tidal influence on seawater intrusion in unconfined coastal aquifers. Water Resour. Res. 48 (2), 1–11.

Langevin, C.D., Thorne, D.T., Dausman, A.M., Sukop, M.C., Guo, W., 2007. SEAWAT Version 4: A Computer Program for Simulation of Multi-Species Solute and Heat Transport: US Geological Survey Techniques and Methods Book 6, (Chapter A22).

Lebbe, L., 1983. Mathematical model of the evolution of the fresh water lens under the dunes and beach with semi-diurnal tides. In: 8th Salt Water Intrusion Meeting, Bari, Geologia Applicata e Idrogeologia, vol. XVIII, parte II. pp. 211–226.

Lebbe, L., 1999. Parameter identification in fresh-saltwater flow based on borehole resistivities and freshwater head data. Adv. Water Resour. 22 (8), 791–806.

Li, X., Hu, B.X., Burnett, W.C., Santos, I.R., Chanton, J.P., 2009. Submarine ground water discharge driven by tidal pumping in a heterogeneous aquifer. Ground Water 47 (4), 558–568.

Mulligan, A.E., Langevin, C., Post, V.E.A., 2011. Tidal boundary conditions in SEAWAT. Ground Water 49 (6), 1–14.

Nielsen, P., 1990. Tidal dynamics of the water table in beaches. Water Resour. Res. 26 (9), 2127–2134.

Nielsen, P., 1999. Groundwater dynamics and salinity in coastal barriers. J. Coastal Res. 15 (3), 732–740.

Niswonger, R.G., Panday, S., Ibaraki, M., 2011. MODFLOW-NWT, A Newton formulation for MODFLOW-2005: US Geological Survey Techniques and Methods 6-A37.

Oude Essink, G.H.P., van Baaren, E.S., de Louw, P.G.B., 2010. Effects of climate change on coastal groundwater systems: a modeling study in the Netherlands. Water Resour. Res. 46 (10), 1–16.

Pauw, P.S., Post, V.E.A., Groen, M.M.A., Groen, J., 2009. The onshore and offshore groundwater salinity distribution between Egmond aan Zee and Castricum aan Zee, MSc. thesis VU University Amsterdam.

Pool, M., Carrera, J., Dentz, M., Hidalgo, J.J., Abarca, E., 2011. Vertical average for modeling seawater intrusion. Water Resour. Res. 47 (11), 1–12.

Post, V.E.A., 2005. Fresh and saline groundwater interaction in coastal aquifers: is our technology ready for the problems ahead? Hydrogeol. J. 13 (1), 120–123.

Reis, A.H., Gama, C., 2010. Sand size versus beachface slope – an explanation based on the Constructal Law. Geomorphology 114 (3), 276–283.

Robinson, C., Gibbes, B., Li, L., 2006. Driving mechanisms for groundwater flow and salt transport in a subterranean estuary. Geophys. Res. Lett. 33 (3), 3–6.

Robinson, C., Li, L., Barry, D.A., 2007. Effect of tidal forcing on a subterranean estuary. Adv. Water Resour. 30 (4), 851–865.

Sulzbacher, H., Wiederhold, H., Siemon, B., Grinat, M., Igel, J., Burschil, T., Günther, T., Hinsby, K., 2012. Numerical modelling of climate change impacts on freshwater lenses on the North Sea Island of Borkum using hydrological and geophysical methods. Hydrol. Earth Syst. Sci. 16 (10), 3621–3643.

Teo, H., Jeng, D.S., Seymour, B.R., Barry, D.A., Li, L., 2003. A new analytical solution for water table fluctuations in coastal aquifers with sloping beaches. Adv. Water Resour. 26 (12), 1239–1247.

Thorn, P., Urish, D., 2012. Preliminary observation of complex salt-fresh water mixing in a beach aquifer. Ground Water 51 (1), 1–6.
Turner, I.L., Coates, B.P., Acworth, 1995. Tides, waves and the super-elevation of groundwater at the coast. J. Coastal Res. 13 (1), 46–60.
Urish, D.W., Melih, M.O., 1989. The coastal ground-water boundary. Ground Water 27 (3), 310–315.
van Dam, J., 1983. The shape and position of the salt water wedge in coastal aquifers. In: Proceedings of the Hamburg Symposium on Relation of Groundwater Quantity and Quality. IAHS 146. pp. 59–75.
Van Meir, N., 2001. Density-Dependent Groundwater Flow: Design of a Parameter Identification Test and 3D-Simulation of Sea-Level Rise. Ph.D. thesis, Ghent University, Ghent.
Vandenbohede, A., Lebbe, L., 2005. Occurrence of salt water above fresh water in dynamic equilibrium in a coastal groundwater flow system near De Panne, Belgium. Hydrogeol. J. 14 (4), 462–472.
Vandenbohede, A., Luyten, K., Lebbe, L., 2008. Effects of global change on heterogeneous coastal aquifers: a case study in Belgium. J. Coastal Res. 24, 160–170.
Viezzoli, A., Tosi, L., Teatini, P., Silvestri, S., 2010. Surface watergroundwater exchange in transitional coastal environments by airborne electromagnetics: the Venice Lagoon example. Geophys. Res. Lett. 37 (1), 1–6.
Werner, A.D., Bakker, M., Post, V.E.A., Vandenbohede, A., Lu, C., Ataie-Ashtiani, B., Simmons, C.T., Barry, D.A., 2013. Seawater intrusion processes, investigation and management: recent advances and future challenges. Adv. Water Resour. 51, 3–26.
Werner, A.D., Gallagher, M.R., 2006. Characterisation of sea-water intrusion in the Pioneer Valley, Australia using hydrochemistry and three-dimensional numerical modelling. Hydrogeol. J. 14 (8), 1452–1469.
Wright, L., Short, A., 1984. Morphodynamic variability of surf zones and beaches: a synthesis. Mar. Geol. 56 (1135), 93–118.
Xin, P., Robinson, C., Li, L., Barry, D.a., Bakhtyar, R., 2010. Effects of wave forcing on a subterranean estuary. Water Resour. Res. 46 (12), 1–17.
Zheng, C., Wang, P.P., 1999. MT3DMS A Modular Three – Dimensional Multispecies Transport Model SA Modular Three-Dimensional Multispecies Transport Model for Simulation of Advection, Dispersion and Chemical Reactions of Contaminants in Ground-Water Systems: Documentation and Users Guide.